Separation and Purification Technology 291 (2022) 120932

Contents lists available at ScienceDirect

Separation and Purification Technology

journal homepage: www.elsevier.com/locate/seppur

Balancing uptake and selectivity in a copper-based metal–organic framework for xenon and krypton separation

Chenghui Zhang [a], Xinglong Dong [b], Yongwei Chen [c,*], Houxiao Wu [d], Liang Yu [d,e], Kang Zhou [e], Ying Wu [d], Qibin Xia [d], Hao Wang [e,*], Yu Han [b], Jing Li [f,e,*]

[a] School of Materials Science and Engineering, University of Jinan, Jinan 250022, People's Republic of China
[b] Advanced Membranes and Porous Materials Center, Physical Sciences and Engineering Division, King Abdullah University of Science and Technology, Thuwal 23955-6900, Saudi Arabia
[c] College of Chemical Engineering, Qingdao University of Science and Technology, Qingdao 266042, People's Republic of China
[d] School of Chemistry and Chemical Engineering, South China University of Technology, Guangzhou 510640, People's Republic of China
[e] Hoffmann Institute of Advanced Materials, Shenzhen Polytechnic, Shenzhen 518055, People's Republic of China
[f] Department of Chemistry and Chemical Biology, Rutgers University, 123 Bevier Road, Piscataway, NJ 08854, United States

ARTICLE INFO

Keywords:
Adsorption separation
Metal–organic frameworks
Xenon
Krypton
Synergetic effect

ABSTRACT

Efficient separation of Xenon (Xe) and krypton (Kr) is important in the gas industries but remains challenging. Adsorptive separation affords an energy-efficient method to isolate the two noble gases, yet developing selective adsorbents with high uptake and excellent selectivity remains difficult, limited by a trade-off between uptake and selectivity. We report MOF-11 with optimal pore size and accessible open metal sites (OMSs) for separation of Xe over Kr via the discriminable difference in van der Waals interactions. MOF-11 affords a new benchmark for Xe/Kr separation with high Xe uptakes of 4.05 and 4.95 mmol/g (at 0.2 and 1 bar), high Xe/Kr Henry and IAST selectivity (13.6 and 16.1) at 298 K. Evidenced by Xe-loaded structure, multiple Xe···H interactions between Xe and the terminal H atoms allow Xe atoms firmly packed within the framework. This work demonstrates a strategy for balancing uptake and selectivity in Xe/Kr separation by capitalizing on the synergy between optimal pore size and OMSs.

1. Introduction

Xenon (Xe) and krypton (Kr) separation is of paramount importance to industry and human life, due to their high demand in many different applications, including medical imaging, spacecraft propellants, insulation, commercial lighting and lasers [1,2]. Xe and Kr are generally obtained from air separation process, however, the concentrations of both gases in air are extremely low (Xe, 0.087 ppm; Kr, 1.14 ppm) [3,4]. Commercially, a 20/80 (v/v) mixture of Xe and Kr is obtained as a byproduct from cryogenic air separation, which then undergoes a second cryogenic distillation to obtain high purity Xe and Kr [5]. It is an uncommon process that requires another cryogenic distillation for isolating pure Xe and Ke, leading to the high prices of both gases, particularly for Xe (approx. $5000/kg) [6]. Besides, Xe and Kr exist in the reprocessed off-gases from used nuclear fuel (UNF) containing radioactive ^{127}Xe (500 ppm) and ^{85}Kr (50 ppm) [7], which must be removed and captured from the off-gas to avoid their emissions to atmosphere, which will cause environment pollution due to their long half-life—most notably radioactive ^{85}Kr ($t_{1/2} = 10.8$ years) [8]. To date, cryogenic distillation remains the most mature technology for Xe/Kr separation. However, such a process is excessively energy-intensive. Accordingly, developing energy-saving alternative separation methods is an urgent task that can efficiently isolate Xe and Kr from air and nuclear waste, finally incentivizing pure Xe and Kr at a reasonable price.

As an alternative method to cryogenic distillation, adsorption-based separation using porous solid adsorbents is regarded as a promising method due to its advantage of economical and energy-efficient feature, which has been broadly studied in the field of gas separation and purification [9–12]. However, due to the weak polarizability (4.04×10^{25} cm^{-3} for Xe and 2.48×10^{25} cm^{-3} for Kr), Xe and Kr atoms are difficult to be polarized by the conventional porous adsorbents. In addition, they have very weak intermolecular interactions (dipole–dipole interaction, π-π stacking, hydrogen bonding) with these adsorbents, limited by the lack of dipole or quadrupole moments [1]. Given the fact that Xe and Kr

* Corresponding authors at: Hoffmann Institute of Advanced Materials, Shenzhen Polytechnic, Shenzhen 518055, People's Republic of China (J. Li).
E-mail addresses: hgchenyongwei@163.com (Y. Chen), wanghao@szpt.edu.cn (H. Wang), jingli@rutgers.edu (J. Li).

https://doi.org/10.1016/j.seppur.2022.120932
Received 7 February 2022; Received in revised form 15 March 2022; Accepted 23 March 2022
Available online 25 March 2022

have very similar kinetic diameters (4.047 Å for Xe and 3.655 Å for Kr with only a 0.392 Å difference), the pore-size matching strategy is also limited [13,14]. Therefore, it is of great challenge to design and construct porous adsorbents for efficient separating Xe from Kr.

In this regard, metal–organic frameworks (MOFs), a promising class of porous crystalline materials, have been investigated in Xe/Kr separation due to their designable chemical functionalities, diverse and customizable structures [15–17]. To date, the primary strategies can be classified into the following categories: ultramicropore [8], open metal sites (OMSs) [18], Ag nanoparticle deposition [19], ions (anions and cations) [20,21], polar functional groups [22], dynamic gate-opening [5], postsynthetic defect healing [23], and metalation [24]. Thallapally et al. [8] reported that SBMOF-1 with diamond-shaped channels of 4.5 Å had a high thermodynamic Xe/Kr selectivity up to 16 at 298 K while the Xe uptakes were relatively low as 1.2 and 1.4 mmol/g at 0.2 and 1 bar, respectively. Li et al. [22] reported a squarate-based MOF with suitable pore size and available polar hydroxyl groups, giving a record Xe/Kr selectivity of 69.7 at 298 K, whereas the Xe uptake was also relatively low (1.35 mmol/g at 1 bar). Xing et al. [5] designed a flexible MOF ZU-62 that can sieve Xe and Kr, benefiting from the rotation of anions and pyridine rings when exposed to larger-size Xe atom. However, the gate-opening pressure toward Xe exceeded 0.2 bar once the temperature increased to room temperature (298 K), which could not meet the actual demand for separating Xe/Kr byproduct from the cryogenic air separation process. Though tremendous effort has been made, ideal adsorbents with both high adsorption capacity and selectivity for the separation of Xe and Kr are yet to be developed.

It is well known that porous adsorbents with both high uptake and selectivity can reduce the energy footprint in gas separations [25]. However, the general trade-off between uptake capacity and selectivity with porous materials is a serious roadblock to the industrial energy-efficient gas separations. As a result, it is highly appreciated to develop ideal MOF adsorbents that have both high Xe uptake amount and excellent Xe/Kr selectivity. To this end, we demonstrate the balancing of the uptake capacity and selectivity for Xe/Kr separation by exploiting the synergetic effect of optimal pore size and OMSs of a microporous MOF. In dehydrated MOF-11 structure, there are two types of channels with oppositely adjacent OMSs and perfect pore sizes matched with Xe atom, thus constructing the proposed the synergetic effect of optimal pore size and OMSs to offer the desired binding sites toward Xe capture. Ultra-high uptake of Xe at low pressure (4.05 mmol/g at 0.2 bar) and good Xe/Kr selectivity at 298 K were simultaneously realized by MOF-11, rendering it a new benchmark for Xe/Kr separation performance.

2. Experimental section

2.1. Synthesis of $Cu_2(ATC)\cdot 6H_2O$.

$Cu_2(ATC)\cdot 6H_2O$ was synthesized following the synthesis protocol previously reported by Yaghi and co-workers [26]. $Cu(NO_3)_2\cdot 3H_2O$ (0.5 mmol, 0.12 g) and H_4ATC (0.25 mmol, 0.078 g) were dissolved in 6 mL aqueous solution of NaOH (60 mg/L) in a 25 mL Teflon-lined autoclave and heated at 190 °C for 24 h. After cooling down to room temperature, green crystals of $Cu_2(ATC)\cdot 6H_2O$ along with small amounts of crystalline H_4ATC were obtained. The green crystals were washed with water and methanol several times to get the pure $Cu_2(ATC)\cdot 6H_2O$ crystals.

3. Results and discussion

The hydrothermal reaction of copper nitrate hydrate and 1,3,5,7-adamantane tetracarboxylic acid (H_4ATC) in basic aqueous solution yielded green crystals of MOF-11 with the formula $Cu_2(ATC)\cdot 6H_2O$. Generally, thermal activation is a prerequisite treatment to evacuate the guest molecules trapped in the pores and coordinated on the metal nodes before gas adsorption. Benefiting from the good crystallinity, the robust structure of dehydrated MOF-11 upon the liberation of water molecules coordinated on each $Cu_2(CO_2)_4$ paddle-wheel unit was crystallized in the tetragonal system with a space group of $P4_2/mmc$ [26]. In the higher symmetry structure of dehydrated MOF-11, each Cu atom in a square geometry is coordinated by four oxygen atoms from four H_4ATC linkers (Fig. 1a), resulting in an OMS on each Cu site due to the removal of one coordinated water molecule. As shown in Fig. 1b, the three-dimensional (3D) framework contains two types of channels with different chemical environments: rectangular pores (termed channel I) with a size of 4.43 × 5.39 $Å^2$ along the *y* axis, and smaller quadrilateral pores (termed channel II) having a short average distance of 3.5 Å along the *y* axis. The channel I is constructed by four oppositely adjacent $Cu_2(CO_2)_4$ paddle-wheel units and the Cu-Cu distance between neighboring paddle-wheel units is only 4.43 Å, possibly providing a strong binging site for Xe nano-trap due to the optimal pore size that is comparable to the kinetic diameter of Xe (4.047 Å) and highly dense OMSs around the inner walls, thereby affording considerable strong interactions due to the synergetic effect of optimal pore size and OMSs in this region. The channel II is assembled by aliphatic hydrocarbon groups of $–CH_2$ and two oppositely adjacent paddle-wheel units. Although the density of OMSs in the channel II is lower than that of the channel I, the combinational presence of low polarity $–CH_2$ groups and oppositely adjacent OMSs can afford another potential binding site for Xe adsorption with strong Xe interaction affinity and high Xe uptake.

Bulk phase purity of the dehydrated MOF-11 was confirmed by powder X-ray diffraction patterns, consistent well with the simulated pattern calculated from the single crystal data (Fig. S1). The permanent porosity of the dehydrated framework was evaluated by N_2 adsorption–desorption isotherms at 77 K (Fig. S2). The calculated Brunauer-Emmett-Teller (BET) and Langmuir areas were 605 and 635 m^2/g, respectively, and the total pore volume was 0.227 cm^3/g for dehydrated MOF-11. Two types of channels in dehydrated MOF-11 were observed in the pore size distributions based on the density functional theory (DFT) method. Thermogravimetric analysis (TGA) revealed that no decomposition of the dehydrated framework occurred below 400 °C under air (Fig. S3). Before 250 ℃, about 20% mass loss was observed due to the adsorbed guest molecules from the open air during the preparation of TGA measurement. Block morphology of MOF-11 was found in the scanning electron microscopy (SEM) image (Fig. S4). Furthermore, this MOF remained good crystallinity and porosity after soaking water for 24 h, as confirmed by the PXRD patterns in Fig. S1 and N2 sorption isotherms in Fig. S5.

It has been well established that MOFs with small channels fairly close to Xe atomic size and accessible OMSs are considered ideal candidates for Xe/Kr separation [16,27,28]. By structural analysis, the synergistic effect of microporous confinement with unique pore environments and high density of OMSs inspires us to evaluate the adsorption performance of Xe and Kr on the dehydrated MOF-11. The sorption isotherms of single-component Xe and Kr at temperatures of 298, 308 and 318 K were measured. As demonstrated in Fig. 2a, MOF-11 exhibits characteristic type I sorption isotherms for Xe atoms with a steep slope in the low pressure range, indicative of strong affinity toward Xe atoms. No hysteresis was observed (Figs. S6-S8) and the saturated Xe uptake amount decreased with the increasing temperature, demonstrating a typical physisorption feature. At 1 bar, the Xe uptakes of MOF-11 were 4.95, 4.79, and 4.55 mmol/g at 298, 308, and 318 K, respectively, with the corresponding packing density of adsorbed Xe estimated to be 2.86, 2.77, and 2.63 g/cm^3, respectively, comparable to the density of liquid Xe (2.94 g/cm^3) at 1 bar and 165 K. At 298 K and 1 bar, the Xe uptake of 4.95 mmol/g is significantly higher than most well-known MOF materials under the same conditions, such as MOF-Cu-H (3.19 mmol/g) [29], squarate-based MOF $Co_3(C_4O_4)_2(OH)_2$ (1.35 mmol/g) [22], CROFOUR-1-Ni (1.78 mmol/g) [20], SBMOF-1 (1.40 mmol/g) [8], ECUT-60 (4.30 mmol/g)[30], ZU-62 (3.30 mmol/g) [5], Ag-MOF-303 (3.35 mmol/g) [24], Ag@MOF-74-Ni (4.80 mmol/g) [19], and is only lower than that of Co_2(*m*-dobdc) (5.99 mmol/g) and Ni_2(*m*-dobdc) (5.58 mmol/g) [3]. In

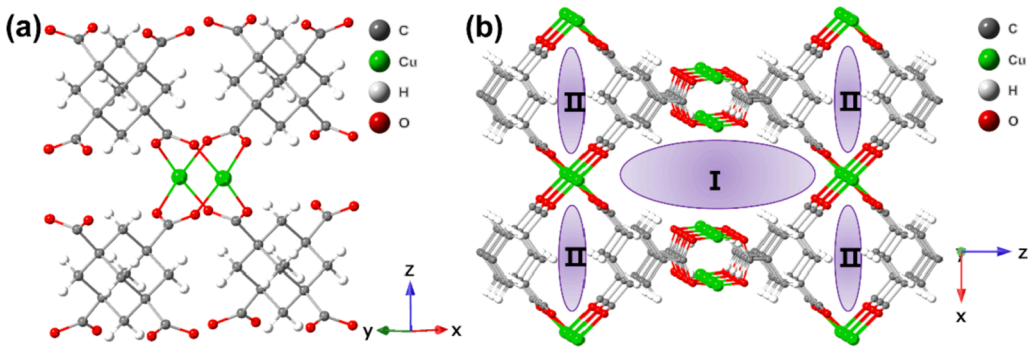

Fig. 1. Crystal structure of dehydrated MOF-11: (a) the coordination environment of Cu node and organic H_4ATC linker, (b) the 3D structure viewed along *y*-axis.

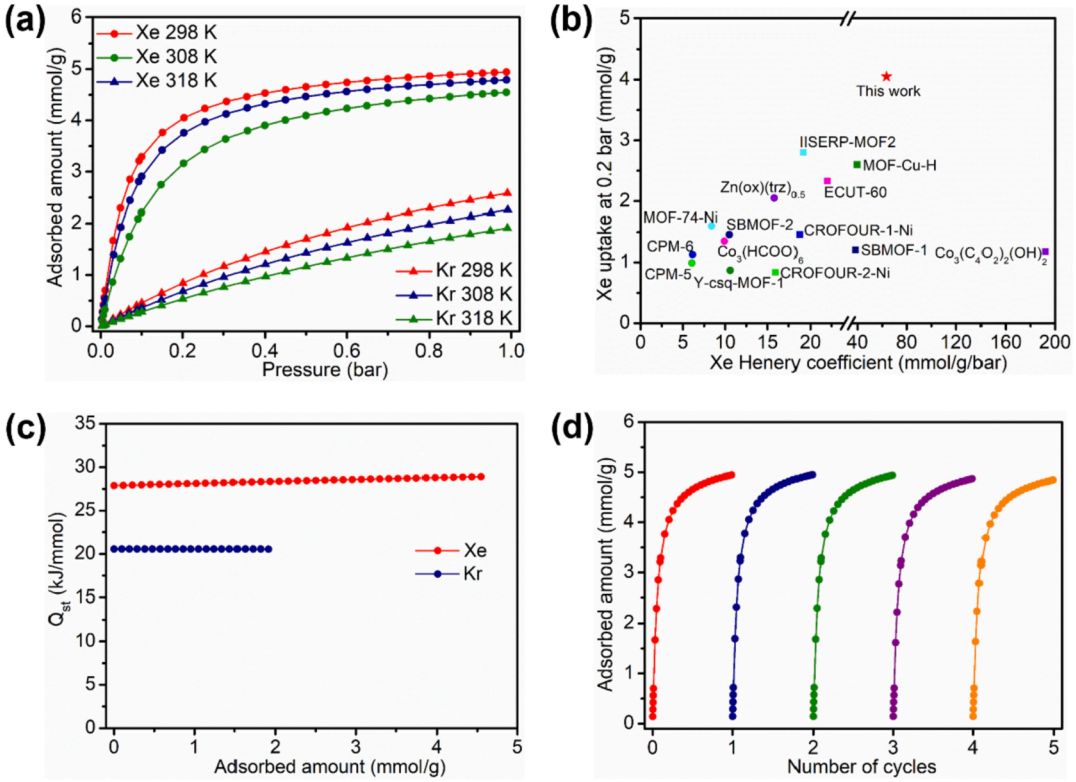

Fig. 2. (a) Xe and Kr sorption adsorption isotherms for MOF-11 at different temperatures. (b) Comparison of Xe uptake at 0.2 bar and Xe Henry coefficient for various materials at 298 K. (c) Q_{st} values of Xe and Kr for MOF-11. (d) Cycling Xe sorption isotherms at 298 K.

contrast, different sorption behavior was observed for Kr. Its adsorption isotherms are almost linear in the measured pressure range (Fig. 2a), suggesting a markedly weaker affinity of this gas toward the MOF sorbent compared to Xe. The Kr uptake capacity of MOF-11 is relatively low with 2.58 mmol/g at 298 K and 1 bar.

Particularly, the uptake of Xe at 0.2 bar is more relevant to the separation of Xe/Kr mixture (20/80, v/v) as this partial pressure most closely reflects the actual conditions of the by-product used in the cryogenic air separation process to produce high purity Xe and Kr [22]. As shown in Fig. 2b, the Xe uptake in MOF-11 reaches 4.05 mmol/g at 298 K and 0.2 bar, which represents the highest value compared all others obtained under the same conditions, making a new benchmark among all reported Xe adsorbent materials. The highest Xe uptake under low pressure ($\leq$0.2 bar) confirms that Xe atoms are efficiently packed in a highly dense mode within the optimal pores.

To evaluate the separation performance of Xe/Kr mixture, we first calculated the Henry selectivity based on Xe and Kr sorption isotherms at low pressure. The Henry coefficient fitting of Xe and Kr sorption isotherms for MOF-11 at 298 K was performed (Figs. S9 and S10) and the accurate Henry constant was then calculated, which is a useful parameter to estimate the adsorbent affinity toward the adsorbate molecules. These values reflect the partition of the adsorbate between its bulk phase and adsorbed phase at extremely low pressure [31]. The corresponding Henry coefficient value was determined to be 63.56 mmol/g/bar for Xe, whereas the corresponding value of Kr was only 4.67 mmol/g/bar, indicating strong affinity of Xe toward MOF-11. To the best of our knowledge, the Henry constant of Xe for MOF-11 is the second highest value for Xe reported so far (Fig. 2b), compared to CROFOUR-1-Ni (18.73 mmol/g/bar) [20], ECUT-60 (22.0 mmol/g/bar) [30], SBMOF-1 (38.42 mmol/g/bar) [8], MOF-Cu-H (39.74 mmol/g/bar) [29], and is only lower than that of the squarate-based MOF $Co_3(C_4O_4)_2(OH)_2$ (192.06 mmol/g/bar) [22]. Consequently, the Henry selectivity was estimated to be 13.6 at 298 K under dilute conditions, which is lower than some top-performing materials such as $Co_3(C_4O_4)_2(OH)_2$ (51.4) [22], CROFOUR-2-Ni (24) [20], IISERP-MOF2 (19.2) [32], and MOF-Cu-H (15.8) [29], but higher than many other Xe adsorbents including

$Co_3(HCOO)_6$ (10.3) [31], SBMOF-2 (9) [33], and UTSA-74 (7.9) [18] as shown in Fig. S11. The high Xe/Kr Henry selectivity indicates the potential of MOF-11 as a sorbent material for industrial separation of Xe and Kr under extremely dilute conditions. The ideal adsorbed solution theory (IAST) was also applied to calculate the selectivity of a binary gas mixture of 20:80 (v/v) Xe/Kr at 298 K. As demonstrated in Fig. S12, the IAST selectivity of MOF-11 was calculated to be 16.1 at 298 K and 1 bar, which is close to the Henry selectivity and significantly higher than some MOFs with OMSs, such as UTSA-74 (8.4) [18], MOF-74-Ni (9) [34], MOF-505 (9) [35], Ni_2(*m*-dobdc) (10.1) [3], Co_2(*m*-dobdc) (11.8) [3], and comparable to the ultra-microporous MOFs including $Zn(ox)_{0.5}(trz)$ (10.2) [36], SB-MOF-1 (16.5) [8], ECUT-60 (11.4) [30], MOF-Cu-H (16.7) [29], and IISERP-MOF2 (18.5) [32]. In addition, the high IAST selectivity places MOF-11 among a group of benchmark MOFs such as ultra-microporous CROFOUR-1-Ni (22) and CROFOUR-2-Ni (15.5) which exhibit synergetic effect between the pore size and CrO_4^{2-} anion [20], Ag@MOF-74-Ni (12) obtained by depositing Ag nanoparticles in MOF-74-Ni [19,33], Cu-MOF-303 (8.2) and Ag-Cu-MOF-303 (10.4) synthesized through the metalation strategy [24], although is still lower than that of the squarate-based MOF $Co_3(C_4O_4)_2(OH)_2$ with the highest selectivity of 69.7 [22]. These results demonstrate that MOF-11 can effectively break the trade-off between uptake capacity and selectivity in adsorptive separation of Xe and Kr by utilizing the synergetic effect of optimal pore size and dense OMSs.

To evaluate the interaction strengths between the MOF framework and the noble gases, the isosteric heats of adsorption (Q_{st}) of Xe and Kr on MOF-11 were calculated by fitting the Xe and Kr sorption isotherms at 298, 308, and 318 K to the Virial equation (Figs. S13 and S14), where the detailed fitting parameters are listed in Table S2. As exhibited in Fig. 2c, the Q_{st} value of Xe for MOF-11 at zero loading was estimated to be 27.9 kJ/mol, higher than that of the corresponding value of 20.6 kJ/mol for Kr, suggesting stronger binding interactions toward Xe compared to Kr in MOF-11 framework, and consequently resulting in selective adsorption of Xe over Kr. We believe this is a result of the optimal pore geometry and high density of accessible OMSs in MOF-11 that is more commensurate with Xe (4.047 Å) than Kr (3.655 Å) [22]. The nearly constant trend in Q_{st} values as a function of loading for both Xe and Kr (Fig. 2c) suggests that the pore environment is energetically homogeneous. To some extent, the relatively low Q_{st} values are beneficial for material regeneration with low energy expenditure. Furthermore, the adsorption–desorption recyclability tests were performed to access the MOF reusability in the Xe sorption. After five consecutive cycles (Fig. 2d), no obvious decrease in Xe uptake was observed, confirming the desirable recycling stability of MOF-11.

To elucidate the interactions between the gases and the framework, molecular simulations were conducted to disclose the adsorption behavior of Xe and Kr in MOF-11 at the molecular level. The optimized Xe and Kr adsorbed configurations were modeled by Metropolis Monte Carlo (MC) method. Both Xe and Kr were trapped in the quadrilateral pore cavities through multiple van der Waals (vdW) interactions between Xe or Kr and H atoms from the aliphatic hydrocarbon inside the pore cavity (Fig. S15), in which the corresponding binding sites located in channel I and II were termed binding sites I and II (Fig. S16). By structural analysis from the three directions of $\times$,*y*, and *z* axes, the binding sites I and II for a nano-trap Xe or Kr were in the same position with the same calculated Xe/Kr···H distances due to the only one orientation of single atom. As expected, nano-trap Xe and Kr occupied nearly the same space whereas Xe sits slightly closer to the MOF framework than Kr. The calculated distances of Xe···H between Xe and the eight terminal H atoms from the H_4ATC ligands are 3.62–4.22 Å with an average Xe···H distance of 3.80 Å, reflecting strong interactions between Xe and the cavity. In contrast, the Kr···H distances range from 3.32 to 4.68 Å with an average distance of 3.88 Å. The calculated shorter distance between Xe and H atom are resulted from the stronger polarizability and lager size of Xe atom. In addition, the binding energy of MOF-11 with Xe was calculated to be 29.19 kJ/mol as a result of energetic favorability, higher than the corresponding value of 20.79 kJ/mol for Kr, with a difference of 8.40 kJ/mol (Fig. S17). The differences in Xe/Kr···H distance and binding energy toward Xr and Kr explains the selective adsorption of Xe over Kr by the benchmark MOF-11.

To directly visualize the location of Xe atoms within MOF-11, the crystal structure of dehydrated MOF-11 after adsorbing Xe atoms was analyzed by single-crystal X-ray diffraction (SCXRD) method. The structure was well refined due to the excellent crystallinity of Xe-loaded MOF-11 sample. In the gas-loaded crystal structure (Fig. 3a), the occupancy of the Xe atoms was determined to be 1.2 per unit cell. The experimental binding sites of Xe are consistent with the results of molecular simulations. Xe atoms are accommodated in the middle of ultra-microporous channels. The multiple vdW interactions between Xe and MOF framework primarily occur through Xe···H between Xe and the terminal H atoms with the shortest distance of 3.37 Å, combined with longer Xe···O distances of 4.17 and 4.26 Å (Fig. 3b and 3c). The average Xe···H distance is 3.74 Å among the twelve H atoms inside the pore wall, comparable to the simulated distance of 3.80 Å. Based on the above experimental and simulated results, the synergetic effect of the optimal pore size and accessible OMSs provides a strong interaction between Xe and the MOF framework by neighboring Xe with multiply H atoms in proximal cavity. Under this condition, the unique nano-trap pores provide high packing density of Xe within MOF-11 as well as high Xe/Kr selectivity. It is noted that during the preparation of this manuscript, Ma and co-workers reported the pores of this framework were smartly self-adjusted for target Xe while remained unchanged for Kr by careful comparison of the distances of between the center and the atom on the vertex within these cavities, as confirmed by the gas-loaded SCXRD measurements [37]. In short, such a combination serves an ideal example of optimal balancing between uptake capacity and selectivity for effective separation of Xe and Kr.

To assess the practical separation performance of MOF-11 for extracting Xe from Xe/Kr mixture, dynamic breakthrough experiments with a mixture of Xe and Kr gases (20/80, v/v, mimicking the composition of the byproduct from cryogenic air separation processes) were conducted under a total flow rate of 2 mL/min at 298 K. About 600 mg sample of dehydrated MOF-11 was packed in a column and initially purged with He at 323 K, and then the Xe/Kr mixture was introduced to pass through the packed column. As shown in Fig. 4, Kr eluted first after 12 min/g due to the weak affinity toward the MOF framework, whereas Xe was not detected until the adsorption of Xe reached saturation with a longer retention time of 82 min/g, demonstrating preferable adsorption of Xe over Kr by MOF-11. The significant difference in the retention time of Xe and Kr confirmed the efficient separation of Xe over Kr realized by MOF-11. In the breakthrough process (Fig. 4), high-purity Kr (>99.9%) could be collected from the outlet effluent with a high productivity of 109 mL/g. Particularly, these values are fairly close to those of high-performance MOFs, including CROFOUR-2-Ni (101 mL/g) [20], MOF-Cu-H (73 mL/g) [29], ECUT-60 (96 mL/g) [30], but lower than ZU-62 (206 mL/g at 273 K) [5]. In addition, due to the lower adsorption heat values for Xe and Kr, Xe and Kr desorption could be facilely implemented by 5 mL/min pure He purge at 323 K (Fig. S18).

4. Conclusions

In conclusion, copper-based MOF-11 exhibits high performance for Xe/Kr separation as a result of its unique structure with optimal pore size comparable to Xe atomic size and high density of accessible OMSs. By virtue of the appropriate aperture and special pore environments, ultra-high Xe uptake of 4.95 mmol/g at 1 bar and at 298 K is achieved. It also has the highest Xe uptake of 4.05 mmol/g at 0.2 bar, the second highest Xe Henry coefficient of 63.56 mmol/g/bar, high Xe/Kr Henry selectivity of 13.6 as well as high IAST Xe/Kr selectivity of 16.1. These results indicate MOF-11 is an ideal Xe adsorbent that can efficiently break the trade-off between the Xe uptake capacity and Xe/Kr selectivity under ambient conditions for the separation of Xe/Kr mixture. The

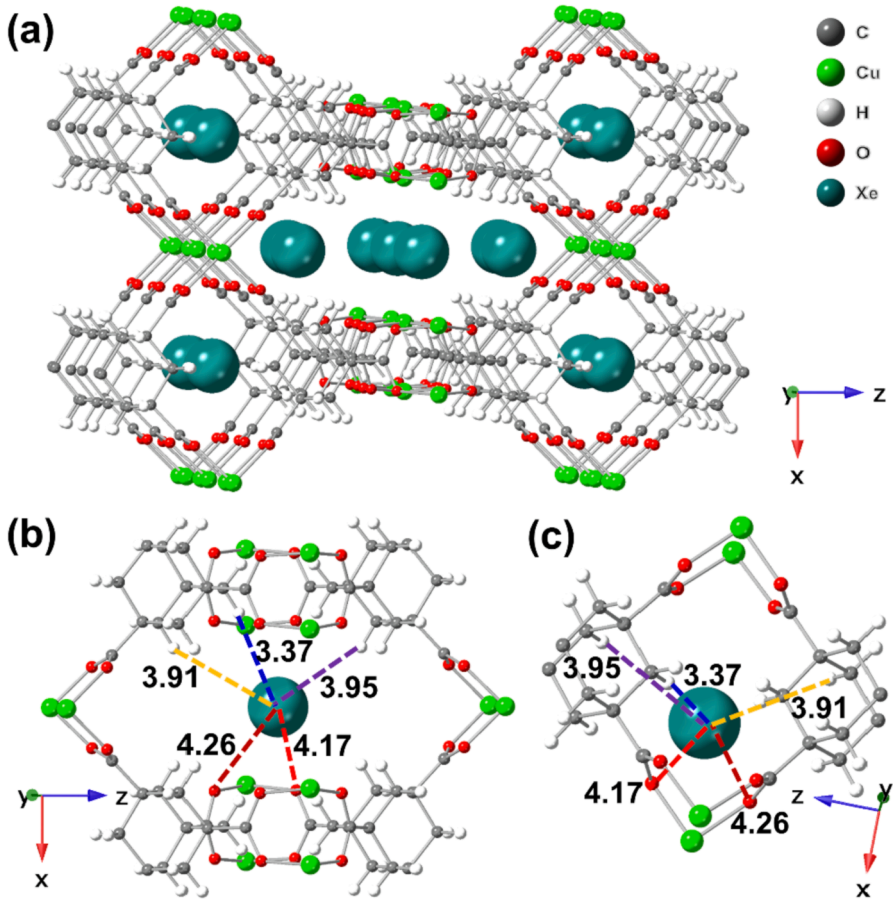

Fig. 3. (a) Single crystal structure of Xe-loaded MOF-11. (b) The binding site in channel I between the adjacent Cu-metal sites and (c) the binding site in channel II in the aliphatic hydrocarbon cavity. The unit of distance is angstrom (Å).

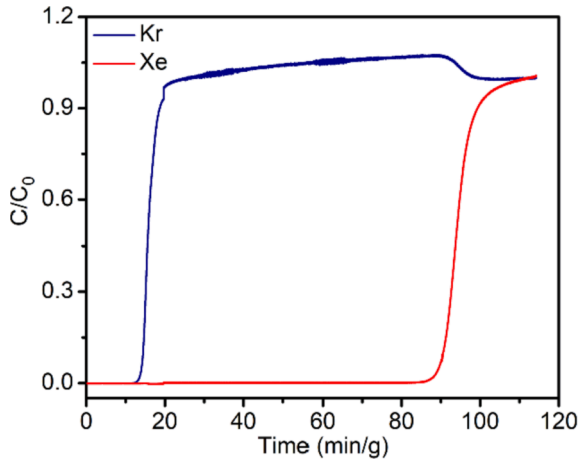

Fig. 4. Breakthrough curves of MOF-11 for a Xe/Kr mixture (20/80, v/v) at 298 K with a flow rate of 2 mL/min.

adsorption sites of MOF-11 for nano-trap Xe can be visualized directly through single crystal structure of Xe-loaded MOF-11 which are further confirmed by theoretical calculations, revealing multiple Xe···H interactions between Xe and the terminal H atoms. Breakthrough experiments demonstrated that MOF-11 could efficiently separate Xe from Xe/Kr mixture with both high uptake and excellent selectivity for Xe. This work provides a good example of MOF-based adsorbents for Xe that offer both high uptake and selectivity to address the challenging Xe/Kr separation by capitalizing on the synergetic effect of optimal pore size and OMSs.

Declaration of Competing Interest

The authors declare that they have no known competing financial interests or personal relationships that could have appeared to influence the work reported in this paper.

Acknowledgements

The authors gratefully acknowledge support from the National Natural Science Foundation of China (Nos. 22108141, 21878101, 21808067, 21706031), Natural Science Foundation of Shandong Province (ZR2021QB013 and ZR2020QB033), Guangdong Natural Science Foundation (2019A1515010692), China Postdoctoral Science Foundation (2018 M640785), Guangdong Basic and Applied Basic Research Foundation (2019A1515011512, 2021A1515010172). Y. Han acknowledges the King Abdullah University of Science and Technology (KAUST) fund for the breakthrough experiments.

Appendix A. Supplementary material

Supplementary data to this article can be found online at https://doi.org/10.1016/j.seppur.2022.120932.

References

[1] F. Chen, J. Ding, K. Guo, L. Yang, Z. Zhang, Q. Yang, Y. Yang, Z. Bao, Y.i. He, Q. Ren, CoNi alloy nanoparticles embedded in metal-organic framework-derived

carbon for the highly efficient separation of xenon and krypton via a charge-transfer effect, Angew. Chem. Int. Ed. Eng. 60 (5) (2021) 2431–2438.
[2] L. Chen, P.S. Reiss, S.Y. Chong, D. Holden, K.E. Jelfs, T. Hasell, M.A. Little, A. Kewley, M.E. Briggs, A. Stephenson, K.M. Thomas, J.A. Armstrong, J. Bell, J. Busto, R. Noel, J. Liu, D.M. Strachan, P.K. Thallapally, A.I. Cooper, Separation of rare gases and chiral molecules by selective binding in porous organic cages, Nat. Mater. 13 (10) (2014) 954–960.
[3] M.T. Kapelewski, J. Oktawiec, T. Runčevski, M.I. Gonzalez, J.R. Long, Separation of xenon and krypton in the metal-organic frameworks M_2(m-dobdc) (M = Co, Ni), Isr. J. Chem. 58 (9-10) (2018) 1138–1143.
[4] S. Xiong, Q. Liu, Q. Wang, W. Li, Y. Tang, X. Wang, S. Hu, B. Chen, A flexible zinc tetrazolate framework exhibiting breathing behaviour on xenon adsorption and selective adsorption of xenon over other noble gases, J. Mater. Chem. A 3 (20) (2015) 10747–10752.
[5] Q. Wang, T. Ke, L. Yang, Z. Zhang, X. Cui, Z. Bao, Q. Ren, Q. Yang, H. Xing, Separation of Xe from Kr with record selectivity and productivity in anion-pillared ultramicroporous materials by inverse size-sieving, Angew. Chem. Int. Ed. Eng. 59 (9) (2020) 3423–3428.
[6] C.M. Simon, R. Mercado, S.K. Schnell, B. Smit, M. Haranczyk, What are the best materials to separate a xenon/krypton mixture? Chem. Mater. 27 (2015) 4459–4475.
[7] J. Li, L. Huang, X. Zou, A. Zheng, H. Li, H. Rong, G. Zhu, Porous organic materials with ultra-small pores and sulfonic functionality for xenon capture with exceptional selectivity, J. Mater. Chem. A 6 (24) (2018) 11163–11168.
[8] D. Banerjee, C.M. Simon, A.M. Plonka, R.K. Motkuri, J. Liu, X. Chen, B. Smit, J. B. Parise, M. Haranczyk, P.K. Thallapally, Metal-organic framework with optimally selective xenon adsorption and separation, Nat. Commun. 7 (2016) 11831.
[9] L. Yang, S. Qian, X. Wang, X. Cui, B. Chen, H. Xing, Energy-efficient separation alternatives: metal-organic frameworks and membranes for hydrocarbon separation, Chem. Soc. Rev. 49 (2020) 5359–5406.
[10] P.M. Bhatt, V. Guillerm, S.J. Datta, A. Shkurenko, M. Eddaoudi, Topology meets reticular chemistry for chemical separations: MOFs as a case study, Chem 6 (2020) 1613–1633.
[11] R.-B. Lin, S. Xiang, W. Zhou, B. Chen, Microporous metal-organic framework materials for gas separation, Chem 6 (2) (2020) 337–363.
[12] Y. Wu, B.M. Weckhuysen, Separation and purification of hydrocarbons with porous materials, Angew. Chem. Int. Ed. 60 (35) (2021) 18930–18949.
[13] Y. Liu, J. Dai, L. Guo, Z. Zhang, Y. Yang, Q. Yang, Q. Ren, Z. Bao, Porous hydrogen-bonded frameworks assembled from metal-nucleobase entities for Xe/Kr separation, CCS Chem. 3 (2021) 1028–1035.
[14] D.C. Fairchild, M.I. Hossain, J. Cordova, T.G. Glover, F.J. Uribe-Romo, Steric and electronic effects on the interaction of Xe and Kr with functionalized zirconia metal-organic frameworks, ACS Mater. Lett. 3 (5) (2021) 504–510.
[15] O.M. Yaghi, M. O'Keeffe, N.W. Ockwig, H.K. Chae, M. Eddaoudi, J. Kim, Reticular synthesis and the design of new materials, Nature 423 (6941) (2003) 705–714.
[16] D. Banerjee, A.J. Cairns, J. Liu, R.K. Motkuri, S.K. Nune, C.A. Fernandez, R. Krishna, D.M. Strachan, P.K. Thallapally, Potential of metal-organic frameworks for separation of xenon and krypton, Acc. Chem. Res. 48 (2) (2015) 211–219.
[17] B.J. Sikora, C.E. Wilmer, M.L. Greenfield, R.Q. Snurr, Thermodynamic analysis of Xe/Kr selectivity in over 137 000 hypothetical metal–organic frameworks, Chem. Sci. 3 (2012) 2217–2223.
[18] Y. Tao, Y. Fan, Z. Xu, X. Feng, R. Krishna, F. Luo, Boosting selective adsorption of Xe over Kr by double-accessible open-metal site in metal-organic framework: experimental and theoretical research, Inorg. Chem. 59 (16) (2020) 11793–11800.
[19] J. Liu, D.M. Strachan, P.K. Thallapally, Enhanced noble gas adsorption in Ag@ MOF-74Ni, Chem. Commun. 50 (4) (2014) 466–468.
[20] M.H. Mohamed, S.K. Elsaidi, T. Pham, K.A. Forrest, H.T. Schaef, A. Hogan, L. Wojtas, W. Xu, B. Space, M.J. Zaworotko, P.K. Thallapally, Hybrid ultra-microporous materials for selective xenon adsorption and separation, Angew. Chem. Int. Ed. 55 (29) (2016) 8285–8289.
[21] B.-y. Liu, Y.-J. Gong, X.-N. Wu, Q. Liu, W. Li, S.-S. Xiong, S. Hu, X.-L. Wang, Enhanced xenon adsorption and separation with an anionic indium–organic framework by ion exchange with Co^{2+}, RSC Ad. 7 (87) (2017) 55012–55019.
[22] L. Li, L. Guo, Z. Zhang, Q. Yang, Y. Yang, Z. Bao, Q. Ren, J. Li, A robust squarate-based metal-organic framework demonstrates record-high affinity and selectivity for xenon over krypton, J. Am. Chem. Soc. 141 (23) (2019) 9358–9364.
[23] K.B. Idrees, Z. Chen, X. Zhang, M.R. Mian, R.J. Drout, T. Islamoglu, O.K. Farha, Tailoring pore aperture and structural defects in zirconium-based metal-organic frameworks for krypton/xenon Separation, Chem. Mater. 32 (9) (2020) 3776–3782.
[24] H. Wang, Z. Shi, J. Yang, T.u. Sun, B. Rungtaweevoranit, H. Lyu, Y.-B. Zhang, O. M. Yaghi, Docking of Cu(I) and Ag(I) in metal-organic frameworks for adsorption and separation of xenon, Angew. Chem. Int. Ed. 60 (7) (2021) 3417–3421.
[25] N. Kumar, S. Mukherjee, N.C. Harvey-Reid, A.A. Bezrukov, K. Tan, V. Martins, M. Vandichel, T. Pham, L.M. van Wyk, K. Oyekan, A. Kumar, K.A. Forrest, K. M. Patil, L.J. Barbour, B. Space, Y. Huang, P.E. Kruger, M.J. Zaworotko, Breaking the trade-off between selectivity and adsorption capacity for gas separation, Chem 7 (11) (2021) 3085–3098.
[26] B. Chen, M. Eddaoudi, T.M. Reineke, J.W. Kampf, M. O'Keeffe, O.M. Yaghi, Cu_2(ATC)·6H_2O: design of open metal sites in porous metal-organic crystals (ATC: 1,3,5,7-adamantane tetracarboxylate), J. Am. Chem. Soc. 122 (2000) 11559–11560.
[27] H. Wang, J. Li, General strategies for effective capture and separation of noble gases by metal-organic frameworks, Dalton Trans. 47 (12) (2018) 4027–4031.
[28] D. Banerjee, C.M. Simon, S.K. Elsaidi, M. Haranczyk, P.K. Thallapally, Xenon gas separation and storage using metal-organic frameworks, Chem 4 (3) (2018) 466–494.
[29] S. Xiong, Y. Gong, S. Hu, X. Wu, W. Li, Y. He, B. Chen, X. Wang, A microporous metal–organic framework with commensurate adsorption and highly selective separation of xenon, J. Mater. Chem. A 6 (11) (2018) 4752–4758.
[30] H. Zhang, Y. Fan, R. Krishna, X. Feng, L.i. Wang, F. Luo, Robust metal–organic framework with multiple traps for trace Xe/Kr separation, Sci. Bull. 66 (11) (2021) 1073–1079.
[31] H. Wang, K. Yao, Z. Zhang, J. Jagiello, Q. Gong, Y.u. Han, J. Li, The first example of commensurate adsorption of atomic gas in a MOF and effective separation of xenon from other noble gases, Chem. Sci. 5 (2) (2014) 620–624.
[32] D. Chakraborty, S. Nandi, R. Maity, R.K. Motkuri, K.S. Han, S. Collins, P. Humble, J.C. Hayes, T.K. Woo, R. Vaidhyanathan, P.K. Thallapally, An ultra-microporous metal-organic framework with exceptional Xe capacity, Chem. Eur. J. 26 (55) (2020) 12544–12548.
[33] X. Chen, A.M. Plonka, D. Banerjee, R. Krishna, H.T. Schaef, S. Ghose, P. K. Thallapally, J.B. Parise, Direct observation of Xe and Kr adsorption in a Xe-selective microporous metal-organic framework, J. Am. Chem. Soc. 137 (22) (2015) 7007–7010.
[34] J.J. Perry, S.L. Teich-McGoldrick, S.T. Meek, J.A. Greathouse, M. Haranczyk, M. D. Allendorf, Noble gas adsorption in metal-organic frameworks containing open metal sites, J. Phys. Chem. C 118 (22) (2014) 11685–11698.
[35] Y.-S. Bae, B.G. Hauser, Y.J. Colón, J.T. Hupp, O.K. Farha, R.Q. Snurr, High xenon/krypton selectivity in a metal-organic framework with small pores and strong adsorption sites, Microporous Mesoporous Mater. 169 (2013) 176–179.
[36] L. Yu, S. Xiong, Y. Lin, L. Li, J. Peng, W. Liu, X. Huang, H. Wang, J. Li, Tuning the channel size and structure flexibility of metal-organic frameworks for the selective adsorption of noble gases, Inorg. Chem. 58 (22) (2019) 15025–15028.
[37] Z. Niu, Z. Fan, T. Pham, G. Verma, K.A. Forrest, B. Space, P.K. Thallapally, A.M. Al-Enizi, S. Ma, Self-Adjusting Metal–Organic Framework for Efficient Capture of Trace Xenon and Krypton, Angew Chem Int Ed 61 (11) (2022).